Available online at www.sciencedirect.com

SciVerse ScienceDirect

Acta Materialia 60 (2012) 5160–5171

Acta MATERIALIA

www.elsevier.com/locate/actamat

Hydrogen embrittlement of ferritic steels: Observations on deformation microstructure, nanoscale dimples and failure by nanovoiding

T. Neeraj [a,*], R. Srinivasan [b], Ju Li [c,d]

[a] ExxonMobil Development Company, Houston, TX 77060, USA
[b] Corporate Strategic Research, ExxonMobil Research and Engineering, Annandale, NJ 08801, USA
[c] Department of Nuclear Science and Engineering, MIT, Cambridge, MA 02139, USA
[d] Department of Materials Science and Engineering, MIT, Cambridge, MA 02139, USA

Received 12 March 2012; received in revised form 5 June 2012; accepted 6 June 2012
Available online 24 July 2012

Abstract

While hydrogen embrittlement of ferritic steels has been a subject of significant research, one of the major challenges in tackling hydrogen embrittlement is that the mechanism of embrittlement is not fully resolved. This paper reports new observations and interpretation of fracture surface features and deformation microstructures underneath the fracture surface, providing a mechanistic view of failure catalyzed by hydrogen. Linepipe grade ferritic steels were tested in air with electrochemically pre-charged hydrogen and in high-pressure H_2 gas. The fracture surface features were studied and compared using high-resolution surface-sensitive scanning electron microscopy, and the deformation microstructures just beneath the fracture surfaces were studied using transmission electron microscopy. Significant dislocation plasticity was observed just beneath both ductile and quasi-brittle fracture surfaces. Further, the dislocation activity just beneath the fracture surfaces was largely comparable with those observed in samples tested without hydrogen. Evidence for hydrogen-enhanced plastic flow localization and shear softening on the sub-micron scale was observed very near the final fracture surface (<2 μm) in the tensile samples. The quasi-brittle fracture surfaces were found to be covered with nanoscale dimples 5–20 nm wide and 1–5 nm deep. Based on analyses of conjugate fracture surfaces, most of the nanodimples appear to be "valley-on-valley" type, rather than "mound-on-valley" type, indicating nanovoid nucleation and growth in the plastically flowing medium prior to ultimate failure. Based on these observations, an alternative scenario of plasticity-generated, hydrogen-stabilized vacancy damage accumulation and nanovoid coalescence as the failure pathway for hydrogen embrittlement is proposed.

Keywords: Hydrogen embrittlement; Transmission electron microscopy; Fracture; Deformation structure; Ferritic steels

1. Introduction

Hydrogen embrittlement of steels is a longstanding technological challenge in the oil and gas industry [1,2]. Recently, hydrogen embrittlement of steels has been considered one of the key challenges in storing and transporting hydrogen for the hydrogen economy [3]. Therefore, it continues to be an active area of research [4–7]. The current understanding of the mechanism of hydrogen embrittlement is that hydrogen from the environment dissolves into steel, migrates as atomic hydrogen towards internal stress centers such as crack tips, and ultimately facilitates nucleation and propagation of cracks, leading to failure [8]. While it is well accepted that hydrogen embrittlement is caused by accumulation of atomic hydrogen at internal centers of high triaxial stresses, the actual micromechanism of failure is not fully understood. Several groups have proposed different mechanisms for hydrogen embrittlement. The three major classes of the proposed mechanisms are

* Corresponding author.
E-mail address: neeraj.s.thirumalai@exxonmobil.com (T. Neeraj).

1359-6454/$36.00 © 2012 Acta Materialia Inc. Published by Elsevier Ltd. All rights reserved.
http://dx.doi.org/10.1016/j.actamat.2012.06.014

hydrogen-enhanced decohesion (HEDE) [9–11], hydrogen-enhanced localized plasticity (HELP) [12,13] and hydrogen-enhanced vacancy stabilization mechanism (VM) [14,15]. In the HEDE mechanism, it is envisioned that hydrogen accumulation at locations of high triaxial stresses leads to weakening of Fe–Fe bonds beyond a critical hydrogen concentration, leading to fracture [9,10]. This implies that any plasticity associated with hydrogen embrittlement is a consequence of the decohesion process and not the direct cause of embrittlement. However, in a series of careful studies, Gerberich and co-workers showed that there is plastic deformation associated with hydrogen embrittlement [11,16]. Using super-dislocation models, Gerberich et al. proposed that dislocations emanating from crack tips greatly enhance local stresses a few nanometers ahead of the crack tip to cause significant hydrogen accumulation (of the order of 50 at.%), which leads to HEDE [11]. The HELP mechanism is supported by in situ transmission electron spectroscopy (TEM) studies, where the introduction of hydrogen gas has been shown to enhance dislocation mobility in many metals and alloys. It was suggested that slip localization such as planar slip may be promoted in the presence of hydrogen, leading to premature fracture. However, the exact micromechanisms of the failure process were not clearly identified in these studies [12,13]. Finally, in the case of the VM model, the primary function of hydrogen in the embrittlement process is envisioned to be the stabilization and promotion of vacancy agglomeration [14,15]. There is indirect experimental evidence suggesting that deformation in the presence of hydrogen can lead to accumulation of excess vacancies in Fe and steel [17,18]. This accumulation of excess vacancies is suggested to lower the ductility in steels that fail through micro-void coalescence (MVC) [14,15]. Despite such a rich literature on both theoretical and experimental work in this area, the actual micromechanism of failure due to hydrogen embrittlement in ferritic steels is still not fully resolved. In the authors' view, there has been little systematic work comparing the deformation microstructures from hydrogen embrittled fracture surfaces (both MVC fracture and quasi-brittle fracture features) with those from samples tested without hydrogen. Further, there have been only a few studies on the nanoscale characterization of the fracture surface features (topography).

Therefore, the primary goal of this work was to characterize the deformation microstructures associated with hydrogen-induced fracture as well as to characterize the fracture surface topography in high resolution to identify the key micromechanisms that lead to hydrogen embrittlement. To this end TEM was employed to study deformation microstructures just underneath fracture surfaces, using focused ion beam (FIB) methods to extract TEM foils. High-resolution scanning electron microscopy (SEM) and atomic force microscopy (AFM) were used to study the nanoscale topographical features on hydrogen-embrittled quasi-brittle facets. Finally, the findings from this work are discussed in relation to prior literature and an alternative nanovoid coalescence (NVC) micromechanism of hydrogen embrittlement for ferritic steels is proposed.

2. Experimental details

In the present work hydrogen embrittlement mechanisms were studied in linepipe grade steels by generating hydrogen-embrittled fracture surfaces by testing in both the hydrogen pre-charged condition and in high-pressure hydrogen gas.

2.1. Materials and hydrogen pre-charged testing

In one set of studies, X65 (yield strength (YS) 448 MPa) and X80 (YS 550 MPa) grade steels were electrochemically pre-charged with 4 wt.ppm of total hydrogen and 1 wt.ppm of diffusible hydrogen using a solution of 5 mg l^{-1} As_2O_3 and 0.5 M H_2SO_4, at a current density of 5 mA cm^{-2} for 4 h. The total hydrogen content was measured with a Leco analyzer. The diffusible hydrogen content was measured using thermal desorption spectroscopy analysis, where all the hydrogen that was evolved up to 300 °C was designated as diffusible hydrogen [19]. Tensile tests on electrochemically pre-charged X65 and X80 steel samples were conducted at a strain rate of 10^{-5} s^{-1} immediately after pre-charging. For the same set of steels, single-edge notched bend (SENB) tests were conducted immediately after electrochemical pre-charging at a K rate of 0.03 MPa $\sqrt{m}$ s^{-1}.

2.2. Materials and testing in gaseous hydrogen

A second set of fracture toughness tests were conducted using compact-tension specimens on X52 (YS 358 MPa), X60 (YS 413 MPa) and X80 (YS 552 MPa) grade linepipe steels in high-pressure H_2 gas under pressures of 5.5 MPa, 21 MPa and 103 MPa. These tests were conducted at Sandia National Laboratories, and tested coupons were provided for this study. Details of this testing and the mechanical properties for these samples are reported elsewhere [20,21].

2.3. Microscopy

The foils for TEM studies were prepared by both standard electropolishing and FIB lift-out techniques using FEI-Helios dual-beam FIB. Electropolishing was performed in a Fischione Model 110 twin-jet electropolishing unit, using a solution of 30 ml perchloric acid (70%), 300 ml methanol and 175 ml butyl alcohol at a temperature of −40 °C. In the FIB lift-out from fracture surfaces, care was taken to prepare foils with the fracture surface preserved (through Pt deposition on the surface) so that one could make deformation microstructure observations from just beneath the fracture surface to several micrometers away from the fracture surface. In the results reported in this work, the thin end of the foil represents the fracture surface. Samples were also prepared for microstructure

analysis of as-received materials using the electropolishing procedure described above and using FIB lift-out. TEM studies were conducted in a Philips CM200 microscope operating at an accelerating voltage of 200 kV. The microstructure analyses were performed using both conventional diffraction contrast techniques and bright-field scanning transmission electron microscopy (BF-STEM) mode. Conventional fractography was performed by SEM in a JEOL 6460-LV microscope with a LaB_6 cathode operated at 15 kV. High-resolution SEM analysis of fracture surface features was performed in a LEO-1530 field emission gun (FEG) at an operating voltage of 3–7 kV with a short working distance of 3–5 mm. AFM observations were performed using an Asylum Research Cypher microscope.

3. Results

3.1. As-received microstructure

The as-received microstructure of the H pre-charged samples is shown in Fig. 1. The X65 linepipe steel had a dual phase ferritic–pearlitic microstructure. The ferrite phase had a grain size of ~10 μm, with a sub-grain size of 1–3 μm (developed during the thermo-mechanical processing of the linepipe). The X80 steel had a ferritic–bainitic microstructure and had ferrite grain size and sub-grain sizes nominally similar to the X65 steel. The as-received sub-grain structure was observed to be the same in TEM foils prepared by both electropolishing and FIB extraction.

The microstructure of samples tested in high-pressure hydrogen gas ranged from ferrite–pearlite to acicular ferrite, depending on the grade of steel, and was previously reported by San Marchi et al. [20,21].

3.2. Fractography and deformation microstructure of hydrogen pre-charged samples

3.2.1. Tensile tested specimens

Tensile tests of electrochemically H pre-charged X65 steel exhibited a decrease in ductility from 15% failure strain for the uncharged condition to 12% failure strain after H pre-charging. Examination of the fracture surfaces by SEM showed that, in both cases, fracture occurred by MVC. There was no apparent change in the failure mode after H pre-charging. In the case of X80 steel, the failure strain was 10% in the uncharged condition and decreased to 8% in the H pre-charged condition. However, in the H pre-charged X80, the fracture mode was significantly altered compared with the uncharged condition. As shown in Fig. 2a, the uncharged X80 steel failed by MVC. However, the H pre-charged X80 exhibited a mixed mode of fracture showing both MVC (on the outside) and quasi-brittle fracture at center of the sample (see Fig. 2b).

Thin foils were then extracted from the fracture surface of tensile coupons using FIB methods to analyze the deformation microstructure associated with the fracture. In the case of X65, the deformation microstructure underneath the MVC fracture regions from both the uncharged and

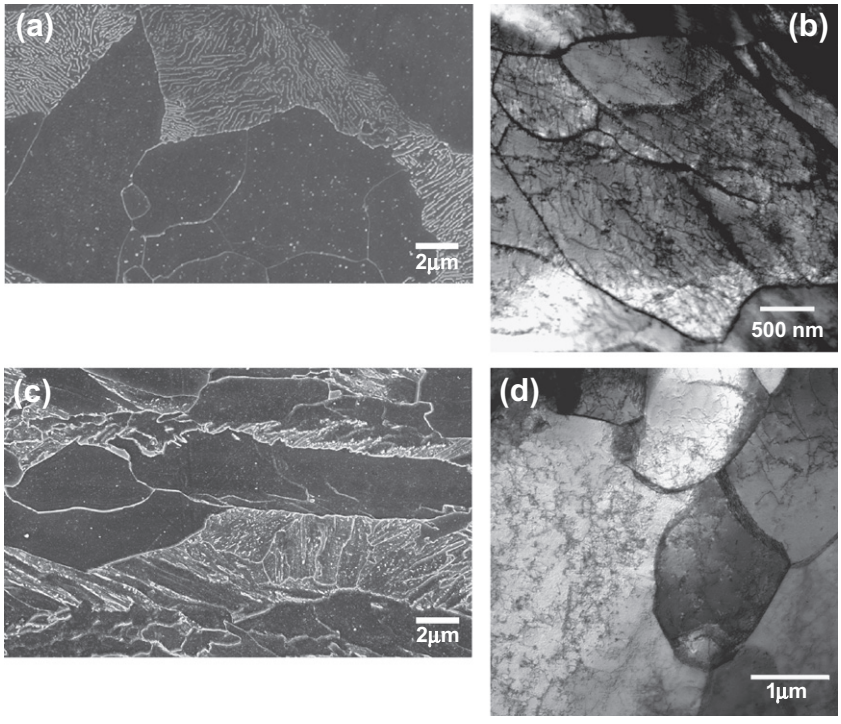

Fig. 1. (a, b) As-received microstructure of X-65 steel used in pre-charged H studies showing ferrite–pearlite microstructure. (c, d) As-received microstructure of X-80 steel used in pre-charged H studies showing ferrite–bainite microstructure.

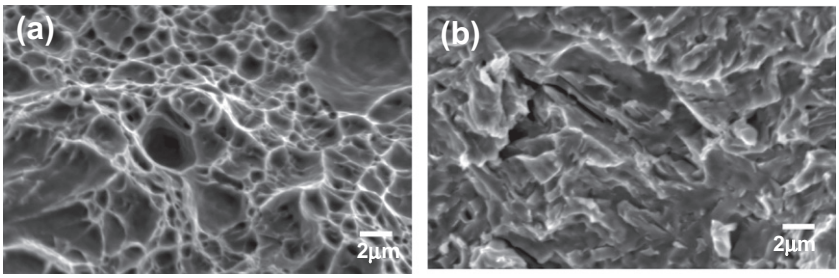

Fig. 2. (a) MVC or ductile fracture observed in uncharged X80 tensile sample. (b) Quasi-brittle fracture observed in H pre-charged X80 tensile sample.

H pre-charged specimens were analyzed. In the case of X80 tensile specimens, observations of deformation microstructure from both MVC fracture regions (both uncharged and H pre-charged condition) and the quasi-brittle fracture regions (in H pre-charged condition) were performed. These results are discussed next.

In Fig. 3a and b, the deformation microstructure beneath the fracture surface of an uncharged X65 MVC fracture is presented. The edge of the foil is the fracture surface and is towards the top in all the micrographs presented in this paper. Thus, these micrographs constitute observations that extend right from the fracture surface to several micrometers below the fracture surface. Key observations from Fig. 3a and b include (a) a very high dislocation density below the fracture surface, indicative of extensive plasticity, and (b) a highly refined sub-grain structure with sub-grain sizes of ~150–300 nm, compared with the starting sizes of 1–3 μm. In some regions, one can observe a series of microvoids of varying sizes nucleating and growing at the sub-grain boundaries (e.g., see Fig. 3b).

The deformation microstructure from H pre-charged X65 is shown in Fig. 3c–e. Again a very high dislocation density and refined sub-grain structure were observed. While the overall deformation microstructure immediately beneath the fracture surface was similar to the uncharged X65, one key difference in the case of the H pre-charged X65 was the observation of dramatic gradation in the sub-grain structure. Superfine sub-grain structures (~50–100 nm) were observed 1–2 μm from the fracture surface (see Fig. 3c and d) which transitioned to coarser (200–300 nm) sub-grains >3 μm away from the fracture surface (Fig. 3e). The significance of these observations is discussed later.

The deformation microstructure from MVC regions of uncharged X80 steel indicated high dislocation density and refined sub-grain structure consistent with the observations made in uncharged X65 steel. The deformation microstructure from a quasi-brittle facet in H pre-charged X80 steel is shown in Fig. 4a and b. Interestingly, this region also showed extensive dislocation plasticity, accompanied by refinement of the sub-grain structure. More significantly, there was a gradation in sub-grain size (indicated by an arrow in Fig. 4a), with very fine sub-grain structure at the fracture surface and coarsening of the structure away from the fracture surface. Fig. 4c and d shows the deformation microstructure beneath a ductile (MVC) fracture region from the same specimen. Again, there was refinement of the sub-grain structure and significant dislocation density indicative of extensive plasticity. Further comparison of the deformation microstructure between MVC (Fig. 4c and d) and quasi-brittle regions (Fig. 4a and b) in H pre-charged X80 steel indicated that they were indistinguishable. To reiterate, the deformation microstructure underneath the fracture surface of both the MVC region

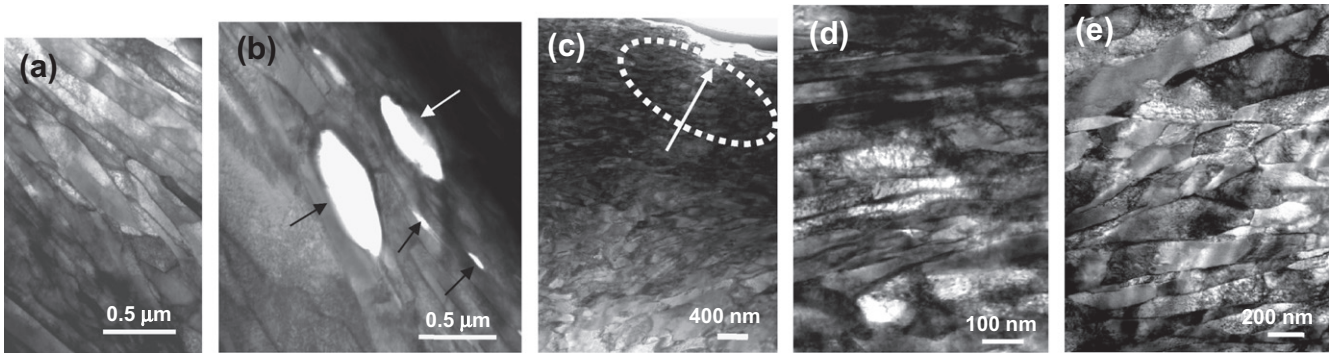

Fig. 3. (a) Deformation microstructure underneath MVC fracture surface showing refined sub-grain structure in uncharged X65 tensile sample. (b) Arrows indicate nucleation of microvoids at sub-grain boundaries in uncharged X65 tensile sample. (c) Microstructure in H pre-charged X65 tensile, indicating strong gradation in sub-grain structure (indicated by arrow). (d) Higher magnification of the marked area in Fig. 3c, showing the very fine sub-grain structure observed underneath the fracture surface. (e) Deformation microstructure from an area ~1 mm away from fracture surface, showing increase in sub-grain size. Note: in all the micrographs, the fracture surface is towards the top of the picture.

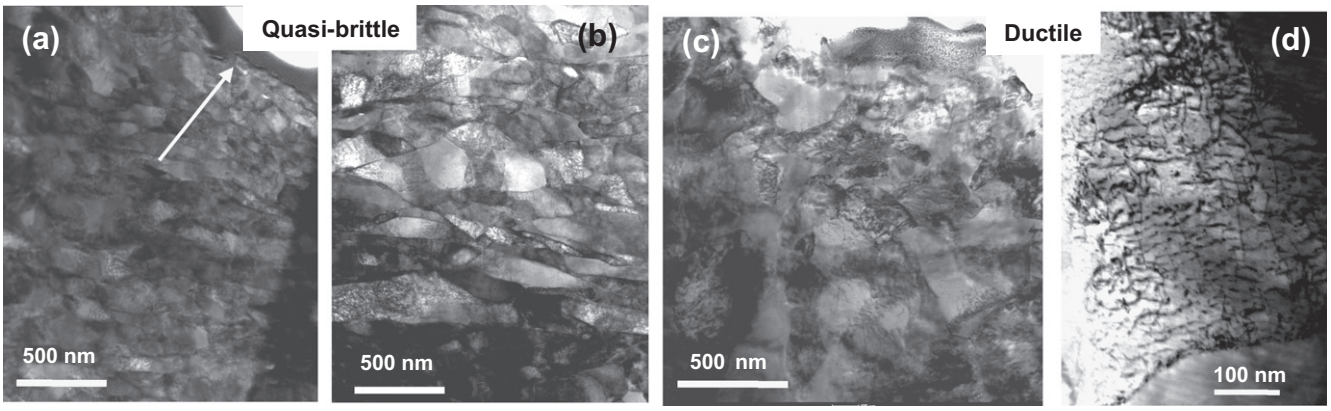

Fig. 4. (a, b) Deformation microstructure underneath quasi-brittle fracture facet in H pre-charged X80 tensile sample showing significant dislocation plasticity leading to refined sub-grain structure. Arrow in Fig. 4a indicates gradation in sub-grain structure, with very fine sub-grains near the fracture surface. (c) Deformation microstructure underneath ductile fracture (MVC) feature in H pre-charged X80 tensile sample. Dislocation plasticity leading to refined sub-grain structure is evident. (d) Dislocation substructure within a sub-grain beneath ductile fracture feature, showing high dislocation density, indicative of significant plasticity.

and the quasi-brittle facet in H pre-charged X80 steel were quite similar and consistent with those observed in H pre-charged X65 steel. This further suggests that, in the presence of hydrogen, significant dislocation plasticity is associated with not only ductile fracture, but also quasi-brittle fracture.

3.2.2. SENB tested specimens

Fractography of uncharged X80 steel in SENB testing showed MVC fracture, while the H pre-charged sample showed quasi-brittle fracture with no evidence of MVC fracture (Fig. 5a). The dislocation structure underneath the fracture surface was studied in both uncharged X80 and H pre-charged X80 steel. In the uncharged X80, there was significant dislocation plasticity with a high dislocation density in a 1–2 μm zone directly beneath the fracture surface, but the as-received sub-grain structure was preserved. As shown in Fig. 5b and c, the deformation microstructure in H pre-charged X80 also exhibited significant plasticity and high dislocation density, with no significant change in the sub-grain structure. Comparing the two conditions, even though the fracture mode changed from MVC to quasi-brittle fracture due to H pre-charging, the underlying deformation microstructure (up to a few micrometers below the fracture surface) remained quite similar and comparable. Studies comparing the uncharged and H pre-charged X65 steel in SENB testing were also conducted, and these results were quite similar and consistent with observations presented for X80 steel above. Finally, it should be noted that the key difference in the deformation microstructure between the tensile and SENB samples was the lack of refined sub-grain structure in the SENB samples.

3.3. Fractography and deformation microstructure of specimens tested in hydrogen gas

When the samples were tested under high-pressure H_2 gas (instead of electrochemically pre-charging with H), conventional fractography indicated that quasi-brittle fracture occurred at all hydrogen gas pressures and in all three grades (X52, X60 and X80) of steels tested. TEM foils were extracted from quasi-brittle facets from X60 samples tested in hydrogen gas pressures of 5.5 MPa, 21 MPa and 103 MPa, respectively. Examples of deformation microstructure underneath the quasi-brittle fracture facets from X60 tested at 5.5 MPa and 103 MPa H_2 gas pressures are shown in Fig. 6. All three samples showed high dislocation

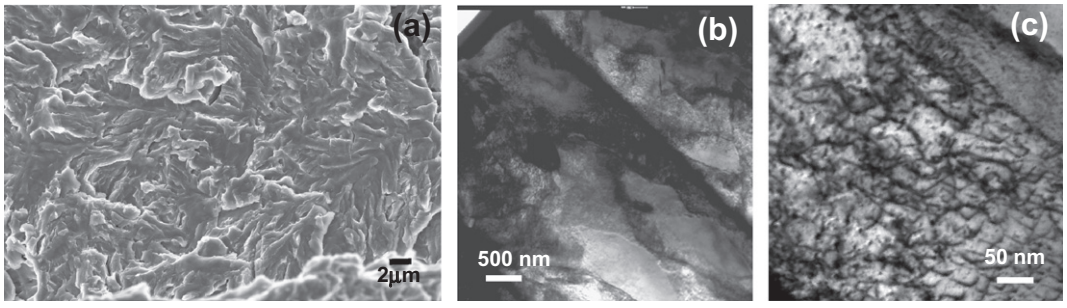

Fig. 5. (a) Quasi-brittle fracture observed in H pre-charged X80 SENB sample. (b, c) Deformation microstructure underneath quasi-brittle facets, indicating significant dislocation plasticity in H pre-charged X80 SENB sample.

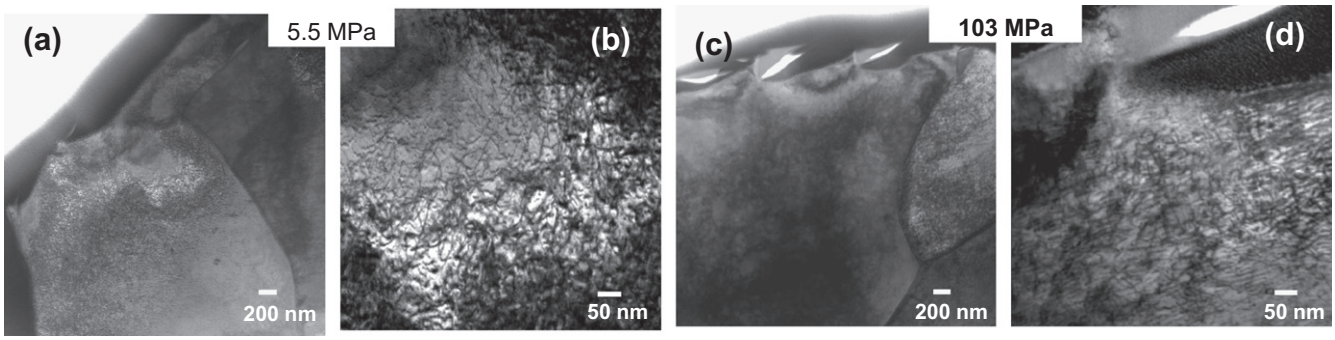

Fig. 6. Deformation microstructure underneath quasi-brittle facets indicating significant dislocation plasticity in X60 CT samples tested in high-pressure hydrogen gas at (a, b) 5.5 MPa and (c, d) 103 MPa.

densities and significant plasticity, with no significant reduction in the sub-grain sizes from the as-received material. There were no apparent differences in the deformation microstructure among the three samples. These results are consistent with the deformation microstructures observed in H pre-charged X65 and X80 steels.

3.4. High-resolution SEM of quasi-brittle fracture facets

The deformation microstructure observations presented above show that there was significant plasticity occurring during hydrogen-induced fracture, whether tested with pre-charged hydrogen or in high-pressure H_2 gas. However, conventional fractography studies indicated quasi-brittle fracture, and there was no apparent evidence yet for manifestation of this plasticity on the fracture surface topography. Further, in the case of X80 tensile studies with pre-charged hydrogen, the deformation microstructure was indistinguishable between a MVC fracture region and a quasi-brittle fracture region immediately beneath the fracture surface. In order to further explore evidence for manifestation of the underlying plasticity, advanced SEM fractography was performed, using imaging conditions more surface sensitive than conventional imaging conditions (see Section 2.3 for details).

Examples of typical quasi-brittle fracture features in hydrogen pre-charged X65 and X80 steels tested in SENB imaged in surface-sensitive imaging conditions are shown in Fig. 7. At low magnifications, the fracture features appear as quasi-brittle facets typically reported in the literature. However, when the quasi-brittle features are imaged at high magnifications, one can observe that the fracture surface exhibits a "mottled" contrast, with dark–bright contrast on the nanometer-scale. Upon close examination, it is apparent that the mottled contrast is due to dense coverage of "nanodimple"-like features on the fracture surface. It is interesting to note that these nanodimples cover the whole fracture surface in samples that fail by quasi-brittle fracture. Further, such nanodimples were also observed on quasi-brittle facets of the pre-charged X80 steel in tensile testing.

High-resolution imaging of quasi-brittle facets was performed on all the samples tested in high-pressure H_2 gas. Again it was observed that the nanodimples were ubiquitous on the fracture surface in all the grades of steel tested (X52, X60 and X80) and for all hydrogen gas pressures. A typical example from X80 steel tested in H_2 gas at a pressure of 21 MPa is shown in Fig. 8.

In order to obtain further evidence that the mottled contrast was produced by features that are due to nanodimples, observations were performed on the same quasi-brittle facet on both halves of the conjugate fracture surfaces. Such analysis of the nanodimple features was conducted on several samples. In Fig. 9, typical examples of conjugate surface analysis from pre-charged X65 steel tested in SENB and from the X80 steel tested in 21 MPa hydrogen gas pressure are shown. Examples of clusters of the same nanodimple features on both halves are circled in Fig. 9. One can observe that these features are not mating pairs with a ligament on one half and dimple on the

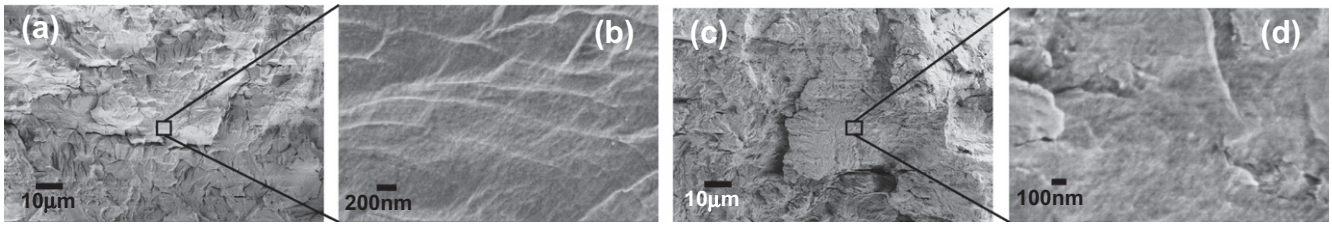

Fig. 7. (a) Typical quasi-brittle fracture observed in H pre-charged X65 SENB sample. (b) Higher magnification view of a small region in Fig. 7a. The fracture surface shows "mottled" contrast, indicating the presence of nanoscale dimples on hydrogen-embrittled quasi-brittle facets. (c) Typical quasi-brittle fracture observed in H pre-charged X80 SENB sample. (b) Higher magnification view of a small region in Fig. 7c. The fracture surface shows "mottled" contrast similar to X65 SENB samples.

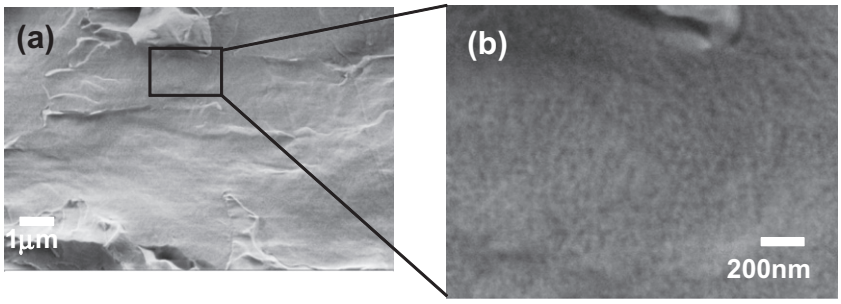

Fig. 8. (a) Typical quasi-brittle fracture observed in X60 CT sample tested in 21 MPa hydrogen gas pressure. (b) Higher magnification view of a small region in Fig. 8a. The fracture surface shows "mottled" contrast, indicating the presence of nanoscale dimples on hydrogen-embrittled quasi-brittle facets. This is similar to the observations in H pre-charged SENB samples.

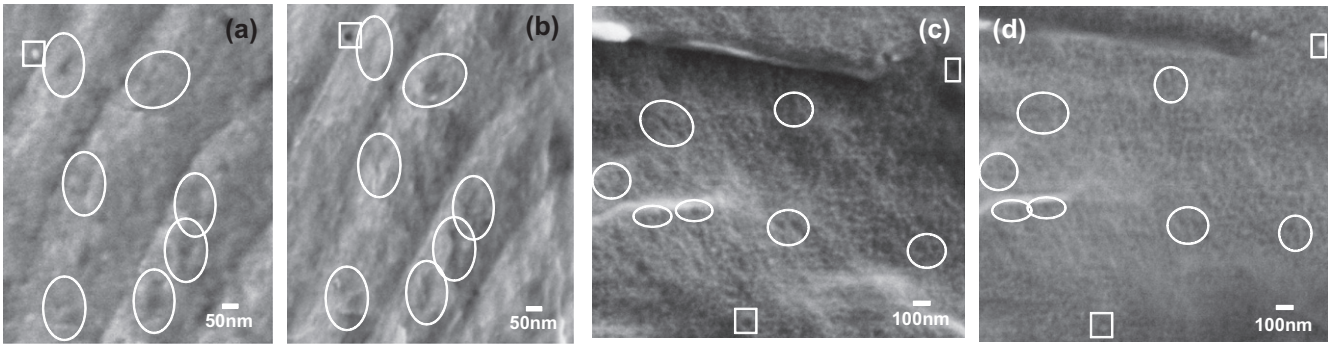

Fig. 9. (a, b) Conjugate surfaces of a quasi-brittle facet in H pre-charged X65 SENB sample. (c, d) Conjugate surfaces of a quasi-brittle facet in X80 CT sample tested under 21 MPa high-pressure hydrogen gas. Both sets of micrographs show that the "mottled" contrast is from nanodimples on quasi-brittle facets. Some of the larger nanodimples or a cluster of nanodimples have been identified by circles/ovals on both halves, showing that they are indeed nanovoids. A few features which represent mating features on conjugate surfaces have been marked with squares. See text for details.

other half. In other words, they appear to be nanodimples on both halves of the conjugate surfaces, and hence are two halves of a nanovoid on the fracture surface. Contrasting this are a few features that were marked with rectangles on both sets of fracture surfaces. These features are mating on the two halves; in other words, what is a void on one half of the sample is a ligament on the other half of the sample. Here, it should be noted that conjugate surface observations of these features are very challenging for a couple of reasons. First, these features are on the nanometer-scale (typically of order 10–20 nm). This makes it quite challenging to identify and locate the same features on conjugate halves of the fracture surface. More importantly, the two halves of the fracture surface can never be mounted in exactly the same orientation for imaging, owing to sample misalignment as well as to the fracture topography itself. For example, in one half of the sample, a feature can be oriented towards the detector and can be imaged well, while in the other half the same feature can be inclined or could be shadowed owing to the fracture surface topography and cannot be imaged under exactly the same orientation and imaging conditions. Taking into consideration these challenges, Fig. 9 still shows that the majority of dimple-like features on the fracture surface would indeed be consistent with nanovoids.

In addition to the SEM studies, limited AFM studies were performed on the pre-charged X65 steel tested in SENB to characterize the surface topography. As shown in Fig. 10, the nanodimple-like features are apparent from

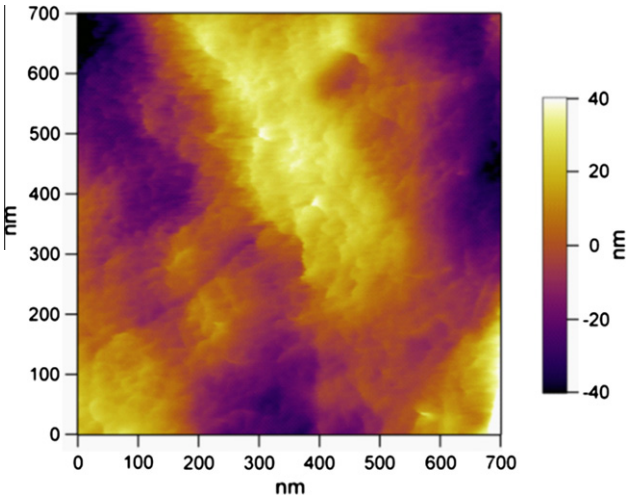

Fig. 10. AFM topography image from a quasi-brittle facet in H pre-charged X65 SENB sample showing the topography from the nanodimples.

the topographical image. Based on preliminary image analysis the nanodimple features ranged in size from 5 to 20 nm; however, they appear to be relatively shallow, with a depth of 1–5 nm. In summary, it appears that the plasticity associated with hydrogen embrittlement in ferritic steels manifests itself as nanodimple like features on the fracture surface.

4. Discussion

In this work, for the first time, comprehensive analysis of the deformation microstructure in hydrogen-embrittled samples was performed, comparing different strength grades, pre-charged hydrogen vs testing in high-pressure H_2 gas, and tensile tests with fracture toughness tests. In this section, these results are discussed in the context of the literature. Further, based on the results of this work, an alternative micromechanism for hydrogen embrittlement in ferritic steels is proposed in the next section.

One of the key observations across the board on all the samples was that there was significant dislocation plasticity immediately beneath the fracture surface in the presence of H, even in samples that show quasi-brittle fracture. As shown in Figs. 3 and 4, the deformation microstructure in the tensile samples indicated very high dislocation density with refinement of the initial sub-grain structure. The authors are not aware of any work in the literature where the deformation microstructures underneath fracture surfaces from tensile tests have been systematically studied with and without hydrogen pre-charging. Strong changes in sub-grain structure are an indication of significant plasticity due to accommodation of shape change of grains during deformation. Observations of refinement of the sub-grain structure have been made in deformation microstructure analysis of rolled metals as well as in situ deformation studies by TEM [22–24]. The observed reduction in sub-grain size starting at 1–3 μm to <300 nm is a clear indication that significant plastic deformation had occurred before final failure in the tensile testing. Further, the fact that this change in sub-grain structure was similar in samples with and without pre-charged hydrogen is an indication that similar deformation processes are operative in both sets of samples. However, one key difference was that, in the pre-charged samples, there was evidence for plastic flow localization very near the final fracture surface (1–2 μm) in both X65 and X80 steels. In the case of the pre-charged X65, one may argue that the conventional necking of ligaments between micro-voids can lead to the superfine sub-grain structure near the final fracture surface. But such a strong gradation in sub-grain structure was not observed in the uncharged X65 sample that also failed by MVC fracture. Also, evidence for plastic flow localization was observed underneath a quasi-brittle fracture facet in the pre-charged X80. Taking into consideration all these observations, it can be stated that there was evidence for hydrogen-enhanced plastic flow localization in the pre-charged tensile samples in the sense that the introduction of pre-charged H must have shear-softened the material on the length scale of several hundred nanometers to a few micrometers close to the eventual fracture plane. While these observations are consistent with proposals of HELP theory [12,13], it is worth noting that there was no direct evidence for slip planarity. Further, the exact microscopic cause(s) for this shear-softening length scale cannot be determined by the current experiments and must await further experimentation and modeling [25].

In the pre-charged SENB samples, both X65 and X80 failed by quasi-brittle fracture. In both cases, there was significant dislocation plasticity, but no apparent evidence for refinement of sub-grain structure. The deformation microstructure of X60 CT samples tested in hydrogen gas at three different gas pressures also showed significant crack-tip plasticity. While there was a qualitative reduction in dislocation density away from the fracture surface in all the fracture toughness samples (both pre-charged and hydrogen gas tested samples), there was no clear evidence for any dramatic gradation in plasticity away from the final fracture surface comparable with the pre-charged tensile samples. While there is little literature available to compare the deformation microstructure observations from hydrogen pre-charged samples, the dislocation structures observed in the high-pressure hydrogen gas tested samples can be compared with those reported recently by Martin et al. [6,7] on a similar linepipe grade steel tested under high-pressure H_2 gas. They also reported significant dislocation plasticity and dense dislocation networks underneath hydrogen-induced quasi-brittle fracture features. While there is no comment on this aspect, based on the published micrographs there was no apparent reduction in sub-grain size close to the fracture surface in their studies either. This means that, if hydrogen-enhanced plastic flow localization and shear softening preceded the eventual failure for these cases, it did not lead to refinement of sub-grain structure. This could be due to the following reasons: for the tensile samples, the shear-softening length scale, damage pattern gradation and the eventual fracture plane are self-evolved from an initially macroscopically uniformly deforming sample that exhibits significant dislocation plasticity. But for the SENB samples, the introduction of an external notch restricted the plasticity to near crack-tip regions, and the amount of plasticity is reduced compared with a tensile sample owing to high stress triaxiality. Therefore, the effects of hydrogen-enhanced plastic flow localization and shear softening could be subtle in the SENB samples, and additional work is needed to establish the length scale.

As discussed in Section 3.4, the quasi-brittle fracture surfaces were characterized at high resolution by SEM for indications of the significant plasticity observed in the TEM studies on the fracture surface. As shown in Figs. 7–10, the most dramatic observation of the hydrogen embrittled quasi-brittle facets was the dense coverage of nanodimples as the final imprint of the fracture process. These nanodimples have been observed in pre-charged

X80 tensile samples that had quasi-brittle facets as well as all the fracture toughness samples for all strength grades examined with either pre-charged hydrogen or those tested in hydrogen gas. Further, as shown in Fig. 9 these nanodimples are apparently due to nanovoids on the fracture surface. The most recent work by Martin et al. [7] reported similar nanodimple-like features being observed in linepipe grade steel tested in high-pressure H_2 gas. However, they have characterized these features as mounds and valleys that occur after the final separation as a result of the relaxation processes associated with the underlying dislocation structure.

Conventional MVC fracture can be thought of as "hole-joining fracture" [26]. There are four main steps in the formation of MVC fracture with this perspective. They are (i) nucleation of voids, (ii) growth and coalescence of voids to form a crack, (iii) extension of the crack by further nucleation and growth of voids ahead of the crack tip and (iv) final separation of the outer rim by shearing [26]. After the final fracture of a MVC process described above, the fracture surface contains dimples as the final signature of the ductile fracture that led to the failure. Analogous to the microvoids/dimples as a signature of "hole-joining fracture" (i.e., a typical ductile fracture) on the micrometer-scale, the nanodimples observed on the quasi-brittle facets of hydrogen embrittled samples can be interpreted as a signature of "hole-joining fracture" at the nanometer-scale. Typically, during MVC fracture in steels, the nucleation of the voids occurs due to interface decohesion or cracking of inclusions or carbides or other hard second-phase particles that are of the order of micrometers in size. These voids will be separated by relatively large distances (several tens or hundreds of micrometers), depending on the microstructure of the material. Hence, for a NVC fracture process, the nanodimple nuclei must be very small. Further, they may need to be very high in density and need to be localized near the eventual fracture surface to be consistent with the experimental observations.

In the last decade Nagumo and co-workers proposed the so-called vacancy model (VM) where it is suggested that the primary function of hydrogen in hydrogen embrittlement is the stabilization and promotion of vacancy agglomeration [14,15]. Sakaki et al. performed positron annihilation studies and provided evidence for excess vacancy accumulation during deformation in the presence of hydrogen [17]. Takai et al. [18] performed a series of interrupted tensile tests in iron and IN625 with hydrogen pre-charging and provided evidence that the "damage" created during deformation in the presence of hydrogen persists even when the diffusible hydrogen is allowed to evolve out of the sample. They attribute this to excess vacancy accumulation during deformation in the presence of hydrogen [18]. However, owing to a lack of microscopy observations, it is unclear how the accumulation of excess vacancies manifests itself in the deformation microstructure and on the fracture surface. Further, Nagumo and co-workers have not proposed a micro-mechanism by which vacancy accumulation can lead to macroscopic fracture (including quasi-brittle fracture).

In the literature, there is extensive discussion on the vacancy mechanism for void nucleation in the areas of ductile fracture in pure metals and radiation-damaged materials [24,27–31]. Cuitino and Ortiz [29] modeled nucleation of voids in pure face-centered cubic metals and suggested that such voids can indeed nucleate and grow to a critical size during quasi-static testing timescales by a diffusive process. They also suggested that these voids could grow by conventional plasticity once they grow to a critical size determined by the inter-dislocation distance (estimated to be 10–30 nm in highly deformed regions). Zinkle et al. [31] performed elasticity calculations on the stability of the vacancy clusters to form voids. Their calculations indicated that the very small voids can only be stable in the presence of gaseous impurities such as O, H and He. More recently, Bringa and co-workers [32–34] published a series of papers on the atomistic mechanism of void growth and suggested that even very small voids (e.g., 2–3 nm) can grow purely by dislocation processes without the need for diffusive processes (if the applied stress is high enough). However, the calculations assume an initial void size of 2–3 nm that has already been nucleated, therefore, do not directly the address the void nucleation process. Based on the available information discussed above, one can reasonably expect that nanovoids can nucleate and grow in the presence of excess vacancies.

Fig. 11 shows a brittle fracture facet from a pre-charged X80 SENB sample that was fractured in liquid nitrogen and imaged under similar conditions. In comparison with Figs. 7–9, it is apparent that the nanodimple-like features are absent in the brittle fracture facet produced by fracturing in liquid nitrogen. This indicates that temperature may play a significant role in the generation of nanodimple features, and therefore it is likely that coupled diffusive–

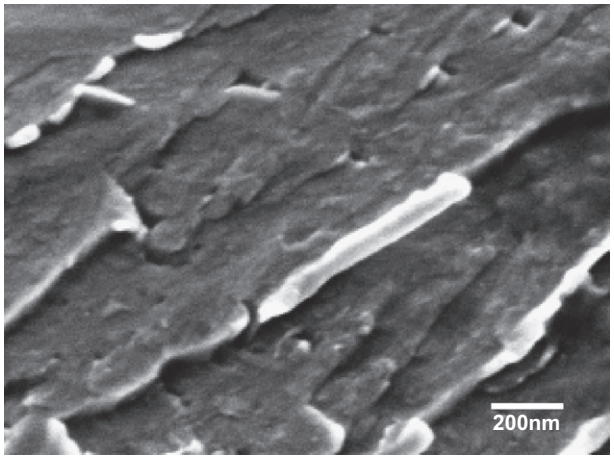

Fig. 11. Micrograph of a brittle facet in X80 generated by fracturing in liquid nitrogen (LN_2). The fracture surface was imaged under conditions similar to those used to reveal the nanodimple structure in hydrogen embrittled quasi-brittle facets. It is clear that the "mottled" contrast and the nanodimples are absent in the LN_2-generated quasi-brittle facet.

displacive processes play a role in the nanovoid nucleation and growth [35,36].

5. NVC micromechanism of hydrogen embrittlement

Based on the observations from this work, an alternative nanovoid nucleation, growth and coalescence micromechanism for hydrogen embrittlement is proposed below and shown schematically in Fig. 12a and b. This mechanism is developed from the point of view that contributions to material toughness from dislocation plasticity are reduced or short-circuited in the presence of hydrogen. This occurs in four stages and leads to fracture with reduction in toughness (or ductility). It is envisioned that initially upon loading in Stage I, the material deforms ahead of the crack tip and starts generating dislocation plasticity. Based on continuum analysis, this plastic zone is initially on the order of 1 mm for a material with a yield strength of 500 MPa and a fracture toughness of 50 MPa $m^{1/2}$ [37]. However, in the presence of hydrogen (either from pre-charging or from high-pressure H_2 gas), hydrogen accumulates in regions of high hydrostatic stresses (e.g., near the crack tip). Furthermore, this hydrogen accumulation can be accentuated by dislocation-assisted convection, as proposed by the HELP mechanism [12,13]. The accumulation of H leads to localization of plasticity within the plastic zone in regions with high local hydrogen content. It leads to Stage II, where intense plasticity occurs in the regions with higher hydrogen concentrations very near the crack tip. This region of localized deformation is designated as the HELP zone and is consistent with HELP theory [12,13]. Based on the TEM observations, this localization of plasticity does not necessarily produce slip bands or planar slip, but rather intense plastic flow localization on the mesoscale. In the case of tensile testing, this plastic flow localization zone is <1 μm, while in the fracture toughness testing it is apparently several micrometers in diameter. It is well known that dislocation plasticity generates excess vacancies [24,27,28,38]. The experimental work of Nagumo and co-workers [17,18] and other first-principles calculations [39,40] have shown that hydrogen binds strongly with vacancies in body-centered cubic Fe. Therefore, in Stage III it is proposed that in the HELP zone next to the crack tip, there is generation and accumulation of excess vacancies that is stabilized by hydrogen binding to the vacancies. A tipping point is reached, through attainment of a critical local excess vacancy concentration that leads to Stage IV, where nucleation and growth of nanovoids occurs, leading to ultimate failure (fracture) by nanovoid coalescence. Such a mechanism can explain the quasi-brittle fracture surface densely covered with nanodimples (typically 5–20 nm). It is also consistent with the previous hydrogen embrittlement theories in that there is a need for critical hydrogen accumulation in a local volume to initiate the failure process, as has been proposed by the HEDE mechanism [9–11]. The resulting plastic flow localization is consistent with the HELP mechanism. Finally, the proposed mechanism provides a micromechanical pathway for failure consistent with the VM proposed by Nagumo [14,15]. Thus, the NVC mechanism implies that, while previously proposed models (HEDE, HELP and VM) can all be operative in the hydrogen-embrittlement process, no single mechanism can

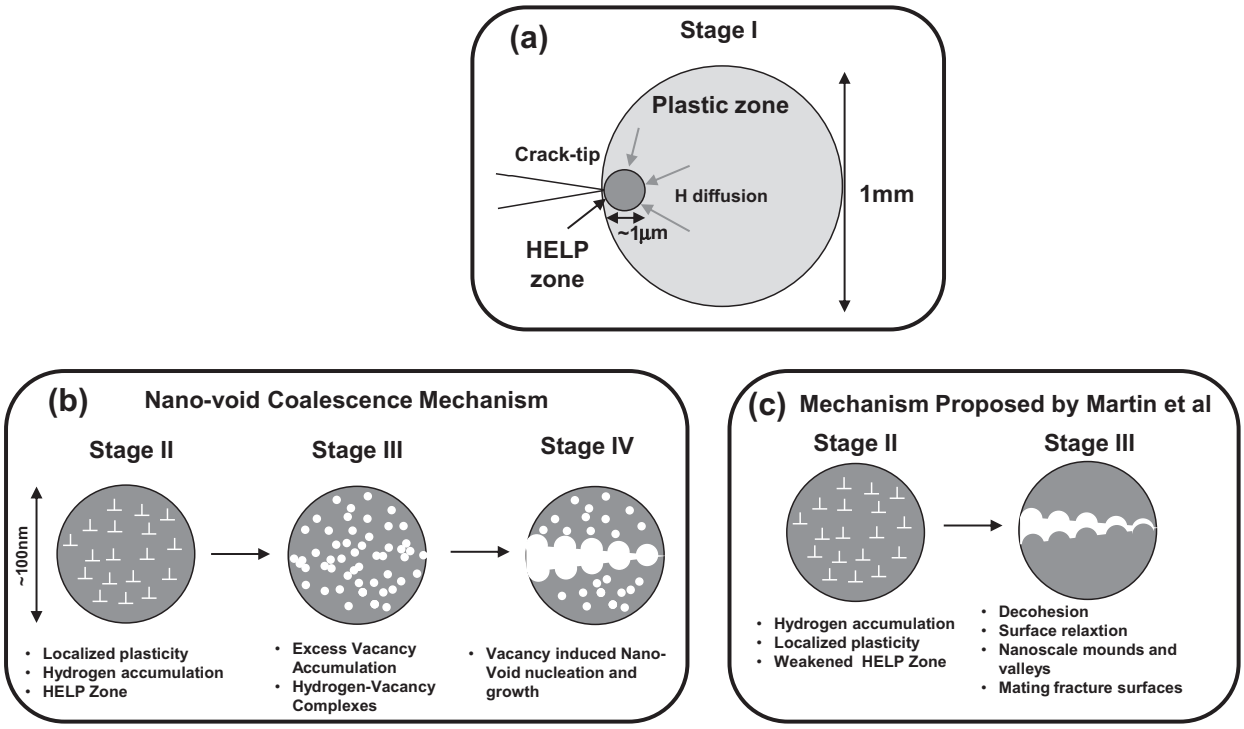

Fig. 12. Schematic of NVC mechanism. See text for details.

completely explain all the associated microstructural features. Rather, the NVC mechanism suggests that a combination of elements of the previously proposed mechanisms is essential for rationalization of the microstructural observations.

Finally, Martin et al. [7] suggested that the evolved deformation microstructure and local hydrogen concentration establish weak regions, which dictate the local crack path and the topology of the fracture surface. This is consistent with the micromechanical processes proposed in this work. However, Martin et al. suggest that the observed nanodimple structure is associated with relaxation processes that occur after final decohesion or separation. As illustrated in Fig. 12c, this would suggest that the conjugate fracture surfaces will be mating surfaces, where a dimple on one face will be a ligament or mound on the opposing face. While there is evidence for such features on the fracture surface, the majority of the features appear to be valleys on both conjugate surfaces (see Fig. 9).

In summary, the proposed plasticity-generated, hydrogen stabilized vacancy damage, vacancy aggregation and NVC mechanism provides a more complete mechanistic and microstructure-based explanation of hydrogen embrittlement in ferritic steels. The exact atomistic processes associated with nanovoid nucleation and growth in hydrogen charged steels needs further investigation. This is currently being pursued by the authors, using atomistic methods, and will be published separately [25].

6. Conclusions

In this work, deformation microstructure and dislocation structure beneath quasi-brittle and MVC regions of fracture surfaces generated in the presence and absence of hydrogen were studied using FIB/TEM methods. Further, the fracture surface topography was studied on the nanometer scale, using FEG-SEM under surface-sensitive imaging conditions and using AFM. Specifically, the following conclusions are drawn from this work.

1. Significant dislocation plasticity has been observed to be associated with hydrogen-embrittlement of ferritic steels. Specifically, there was evidence of sub-grain structure refinement underneath MVC regions and dense dislocation networks underneath quasi-brittle facets in linepipe grade ferritic steels fractured under a variety of testing conditions. These include tensile and fracture toughness testing with either pre-charged hydrogen or in high-pressure H_2 gas.
2. There was evidence for hydrogen-enhanced plastic flow localization at the mesoscale in the presence of hydrogen, especially in tensile tested samples.
3. High-resolution SEM studies of conjugate fracture surfaces of quasi-brittle facets provide evidence for fracture due to nanovoids in the presence of hydrogen. This manifests as nanoscale (10–20 nm) dimples on the fracture surface.
4. By means of fracture surface and microstructural observations, an alternative micromechanism based on plasticity-generated, hydrogen-stabilized vacancy damage and vacancy-induced nanovoid nucleation and coalescence (NVC) is proposed as the failure mechanism leading to quasi-brittle fracture in the presence of hydrogen in ferritic steels.

Acknowledgments

The authors acknowledge the help of Dr Ramgopal Thodla of DNV for performing the electrochemical precharging and mechanical testing of the X65 and X80 samples. They also appreciate and acknowledge the tremendous help of Dan Huber of The Ohio State University in preparing the FIB foils from the difficult fracture surfaces. T.N. would like to thank Dr Brian Somerday at Sandia National Laboratories, Livermore, CA, for providing the high-pressure H_2 gas tested specimens. J.L. would like to acknowledge financial support by ExxonMobil Research and Engineering and partial support by NSF CMMI-0728069. Finally, the authors would like to thank Dr Dalia Yablon of Corporate Strategic Research, ExxonMobil Research and Engineering for performing the AFM studies.

References

[1] Merrick RD. Mater Perform 1989;28:53–5.
[2] Rhodes PR, Skogsberg LA, Tuttle RN. Corrosion 2007;63:63–100.
[3] Somerday BP, Sofronis P, Jones R. Effects of hydrogen in materials. Jackson Hole (WY): ASM International; 2009.
[4] Song J, Curtin WA. Acta Mater 2011;59:1557–69.
[5] Barnoush A, Vehoff H. Acta Mater 2010;58:5274–85.
[6] Martin ML, Fenske JA, Liu GS, Sofronis P, Robertson IM. Acta Mater 2011;59:1601–6.
[7] Martin ML, Robertson IM, Sofronis P. Acta Mater 2011;59:3680–7.
[8] Hirth JP. Metall Trans A 1980;11:861–90.
[9] Troiano AR. Trans Am Soc Met 1960;52:54–80.
[10] Oriani RA. Corrosion 1987;43:390–7.
[11] Gerberich WW, Oriani RA, Lii M-J, Chen X, Foecke T. Philos Mag A 1991;63:363–76.
[12] Birnbaum HK, Sofronis P. Mater Sci Eng, A 1994;176:191–202.
[13] Robertson IM, Lillig D, Ferreira PJ. In: Somerday BP, Sofronis P, Jones R, editors. Hydrogen in metals. Jackson Hole (WY): ASM International; 2009.
[14] Nagumo M. ISIJ Int 2001;41:590–8.
[15] Nagumo M. Mater Sci Technol 2004;20:940–50.
[16] Gerberich WW, Stauffer DD, Sofronis P. In: Somerday BP, Sofronis P, Jones R, editors. Effects of hydrogen on materials. Proceedings of the 2008 international hydrogen conference. Jackson Hole (WY): ASM International; 2009. p. 38–45.
[17] Sakaki K, Kawase T, Hirato M, Mizumo M, Araki H, Shirai Y, et al. Scripta Mater 2006;55:1031–4.
[18] Takai K, Shoda H, Suzuki H, Nagumo M. Acta Mater 2008;56:5158–67.
[19] Srinivasan R, Neeraj T. Unpublished research.
[20] San Marchi C, Somerday BP, Nibur KA, Stalheim DG, Boggess T, Jansto S. PVP2010. Bellevue (WA): ASME; 2010. p. 25825.
[21] San Marchi C, Somerday BP, Nibur KA, Stalheim DG, Boggess T, Jansto S. PVP2011. Baltimore (MD): ASME; 2011. p. 57684.
[22] Hansen N, Juul Jensen D. Mater Sci Technol 2011;27:1229–40.

[23] Hughes DA, Hansen N. Acta Mater 1997;45:3871–86.
[24] Wilsdorf HGF. Mater Sci Eng 1983;59:1–39.
[25] Li S, Li J, Neeraj T, Srinivasan R. Unpublished research.
[26] Hull D. Fractography: observing, measuring and interpreting fracture surface topography. Cambridge: Cambridge University Press; 1999.
[27] Lyles Jr RLW. Acta Metall 1975;23:269–77.
[28] Wilsdorf HGF. Acta Metall 1982;30:1247–58.
[29] Cuitino AM, Ortiz M. Acta Mater 1996;44:427–36.
[30] Farrell K. Radiat Eff 1980;53:175–94.
[31] Zinkle SJ, Wolfer WG, Kulcinski GL, Seitzman LE. Philos Mag A 1987;55:127–40.
[32] Bringa EM, Traiviratana S, Meyers MA. Acta Mater 2010;58:4458–77.
[33] Tang Y, Bringa EM, Remington BA, Meyers MA. Acta Mater 2011;59:1354–72.
[34] Traiviratana S, Bringa EM, Benson DJ, Meyers MA. Acta Mater 2008;56:3874–86.
[35] Zhu T, Li J. Prog Mater Sci 2010;55:710–57.
[36] Wang YZ, Li J. Acta Mater 2010;58:1212–35.
[37] Suresh S. Fatigue of materials. 2nd ed. Cambridge: Cambridge University Press; 1998.
[38] Wu YC, Teng MK, Hsia Y, Chang XR, Tian ZZ, Hsiao CM. Mater Sci Forum 1995;175–178:573–6.
[39] Desai SK, Neeraj T, Gordon PA. Acta Mater 2010;58:5363–9.
[40] Tateyama Y, Ohno T. Phys Rev B 2003;67:174105.